

# PoseCNN: A Convolutional Neural Network for 6D Object Pose Estimation in Cluttered Scenes

Yu Xiang, Tanner Schmidt, Venkatraman Narayanan and Dieter Fox

**Abstract**—Estimating the 6D pose of known objects is important for robots to interact with objects in the real world. The problem is challenging due to the variety of objects as well as the complexity of the scene caused by clutter and occlusion between objects. In this work, we introduce a new Convolutional Neural Network (CNN) for 6D object pose estimation named PoseCNN. PoseCNN estimates the 3D translation of an object by localizing its center in the image and predicting its distance from the camera. The 3D rotation of the object is estimated by regressing to a quaternion representation. PoseCNN is able to handle symmetric objects and is also robust to occlusion between objects. In addition, we contribute a large scale video dataset for 6D object pose estimation named the YCB-Video dataset. Our dataset provides accurate 6D poses of 21 objects from the YCB dataset [1] observed in 92 videos with 133,827 frames. We conduct experiments on our YCB-Video dataset and the OccludedLINEMOD dataset [2] to show that PoseCNN provides very good estimates using only color as input.

## I. INTRODUCTION

Recognizing objects and estimating their poses in 3D has wide applications in many robotic tasks. For instance, recognizing the 3D location and orientation of objects is important for robot manipulation. It is also useful in human-robot interaction tasks such as learning from demonstration. However, the problem is challenging due to the variety of objects in the real world. They have different 3D shapes, and their appearances on images are affected by lighting conditions, clutter in the scene and occlusion between objects.

Traditionally, the problem of 6D object pose estimation is tackled by matching feature points between 3D models and images [3], [4], [5]. However, these methods require that there are rich textures on the objects in order to detect feature points for matching. As a result, they are unable to handle texture-less objects. With the emergence of depth cameras, several methods have been proposed for recognizing texture-less objects using RGB-D data [6], [7], [8], [9]. For template-based methods [6], [10], occlusion significantly reduces the recognition performance. Alternatively, methods that perform learning to regress image pixels to 3D object coordinates in order to establish the 2D-3D correspondences for 6D pose estimation [7], [11], cannot handle symmetric objects well.

In this work, we propose a generic framework for 6D object pose estimation where we attempt to overcome the limitations of existing methods. We introduce a novel Convolutional Neural Network (CNN) for end-to-end 6D pose

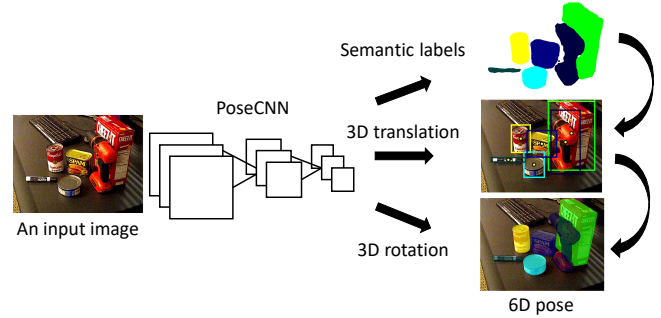


Fig. 1. We propose a novel PoseCNN for 6D object pose estimation, where the network is trained to perform three tasks: semantic labeling, 3D translation estimation, and 3D rotation regression.

estimation named PoseCNN. The novelty of our network lies in that it decouples the estimation of the 3D rotation  $\mathbf{R}$  and the 3D translation  $\mathbf{T}$ , where we employ the observation that  $\mathbf{T}$  can be recovered from the location and scale of the object on the image and  $\mathbf{R}$  can be estimated from the image appearance of the object. Specifically, PoseCNN performs three related tasks as illustrated in Fig. 1. First, it predicts an object label for each pixel in the input image. Second, it estimates the projection of  $\mathbf{T}$  on the image, i.e., 2D object center, by predicting a unit vector from each pixel towards the center. Using the semantic labels, image pixels associated with an object vote the object center location on the image. In addition, the network also estimates the distance of the center. Assuming known camera intrinsics, estimation of the 2D object center and its distance enables us to recover  $\mathbf{T}$ . Finally, the 3D Rotation  $\mathbf{R}$  is estimated by regressing convolutional features extracted inside the bounding box of the object to a quaternion representation of  $\mathbf{R}$ . The rotation regression and the 2D center voting for estimating  $\mathbf{R}$  and  $\mathbf{T}$  can be applied to textured/texture-less objects and symmetric/non-symmetric objects. More importantly, the center voting is robust to occlusion since the network is trained to vote on occluded centers as well.

Another contribution of this work is that we collected a large scale RGB-D video dataset for 6D object pose estimation named the YCB-Video dataset. Our dataset contains 21 objects from the YCB object and model set [1] in 92 videos with a total of 133,827 frames, which is two full orders of magnitude larger than the LINEMOD dataset [6] widely used for 6D pose estimation. Ground truth object poses are provided for every frame. To achieve this, we first manually initialize the object poses on the first video frame, and then use a model-based object tracking system to estimate the camera trajectory and subsequent poses of

Yu Xiang, Tanner Schmidt and Dieter Fox are with the Paul G. Allen School of Computer Science & Engineering, University of Washington, Seattle, WA 98195, USA {yuxiang, tws10, fox}@cs.washington.edu

Venkatraman Narayanan is with the Robotics Institute at Carnegie Mellon University, Pittsburgh, PA 15213, USA venkatraman@cs.cmu.edu

objects. The objects in our dataset are arranged in various poses and spatial configurations, and there is severe occlusion between objects, which makes it a useful and challenging dataset for 6D pose estimation.

In order to evaluate our method, we conduct experiments on both our YCB-Video dataset and the OccludedLINEMOD dataset introduced in [2]. Since both datasets contain depth images, we can refine the poses predicted from PoseCNN with the Iterative Closest Point (ICP) algorithm. We also experiment with using stereo image pairs and multi-view images in the YCB-Video dataset to perform pose refinement. We achieve comparable results as the state-of-the-art methods on the OccludedLINEMOD dataset and provide extensive analyses on our YCB-Video dataset.

This paper is organized as follows. After discussing related work, we introduce PoseCNN for 6D object pose estimation, followed by experimental results and a conclusion.

## II. RELATED WORK

6D object pose estimation methods in the literature can be roughly classified into template-based methods and feature-based methods.

In template-based methods, a rigid template is constructed and used to scan different locations in the input image. At each location, a similarity score is computed, and the best match is obtained by comparing these similarity scores [10], [6], [12]. In 6D pose estimation, a template is usually obtained by rendering the corresponding 3D model. Template-based methods are useful in detecting texture-less objects. However, in order to handle pose variations, a large number of templates are needed, which increases the running time. In addition, template-based methods cannot handle occlusion very well, since the template will have low similarity score if the object is occluded.

In feature-based methods, local features are extracted from either points of interest or every pixel in the image and matched to features on the 3D models to establish the 2D-3D correspondences, from which 6D poses can be recovered [3], [4], [13]. Feature-based methods are able to handle occlusions between objects. However, they require sufficient textures on the objects in order to compute the local features. To handle texture-less objects, a few approaches have been proposed to directly regress to 3D object coordinate location for each pixel to establish the 2D-3D correspondences [7], [2], [11]. But 3D coordinate regression encounters ambiguities in dealing with symmetry objects.

In this work, we achieve the advantages of both template-based methods and feature-based methods in a deep learning framework for 6D object pose estimation, where the network combines bottom-up pixel-wise labeling with top-down object pose regression. Recently, the 6D object pose estimation problem receives more attentions thanks to the competition in the Amazon Picking Challenge (APC). Several datasets and approaches have been introduced for the specific setting in the APC [14], [15]. Our network has the potential to be applied to the APC setting as long as the appropriate training data is provided.

## III. POSECNN

Given an input image, the task of 6D object pose estimation is to estimate the rigid transformation from the object coordinate system  $O$  to the camera coordinate system  $C$ , where we assume that the 3D model of the object is available and the object coordinate system is defined in the 3D space of the model. The rigid transformation here consists of a 3D rotation  $\mathbf{R}(\alpha, \beta, \gamma)$  and a 3D translation  $\mathbf{T} = (T_x, T_y, T_z)^T$ , where  $\alpha$ ,  $\beta$  and  $\gamma$  denote the rotation angles around the  $X$ -axis,  $Y$ -axis and  $Z$ -axis of the the object coordinate system  $O$ , respectively, and  $\mathbf{T}$  is the coordinate of the origin of  $O$  in the camera coordinate system  $C$ . As we can see, the object pose has 6 degrees of freedom and lies in the Special Euclidean group  $SE(3)$ .

In the imaging process,  $\mathbf{T}$  determines the object location and scale in the image while  $\mathbf{R}$  affects the image appearance of the object according to the 3D shape and texture of the object. Since these two parameters have distinct visual properties, we propose a convolutional neural network architecture that internally decouples the estimation of  $\mathbf{R}$  and  $\mathbf{T}$  for 6D object pose estimation.

### A. Overview of the Network

Fig. 2 illustrates the architecture of our network for 6D object pose estimation. The network contains two stages. The first stage consists of 13 convolutional layers and 4 max-pooling layers, which extract feature maps with different resolutions from the input image. This stage is the backbone of the network since the extracted features are shared across all the tasks performed by network. The second stage consists of an embedding step that embeds the high-dimensional feature maps generated by the first stage into low-dimensional, task-specific features. Then, the network performs three different tasks that lead to the 6D pose estimation, i.e., semantic labeling, 3D translation estimation, and 3D rotation regression as described next.

### B. Semantic Labeling

In order to detect objects in images, we resort to semantic labeling, where the network classifies each image pixel into an object class. Compared to object detection methods using bounding boxes [16], [17], semantic labeling provides richer information about the objects and handles occlusion better.

The embedding step of the semantic labeling branch, as shown in Fig. 2, takes two feature maps with channel dimension 512 generated by the feature extraction stage as inputs. The resolutions of the two feature maps are  $1/8$  and  $1/16$  of the original image size, respectively. The network first reduces the channel dimension of the two feature maps to 64 using two convolutional layers. Then it doubles the resolution of the  $1/16$  feature map with a deconvolutional layer. After that, the two feature maps are summed and another deconvolutional layer is used to increase the resolution by 8 times in order to obtain a feature map with the original image size. Finally, a convolutional layer operates on the feature map and generates semantic labeling scores for pixels. The output of this layer has  $n$  channels with  $n$  the

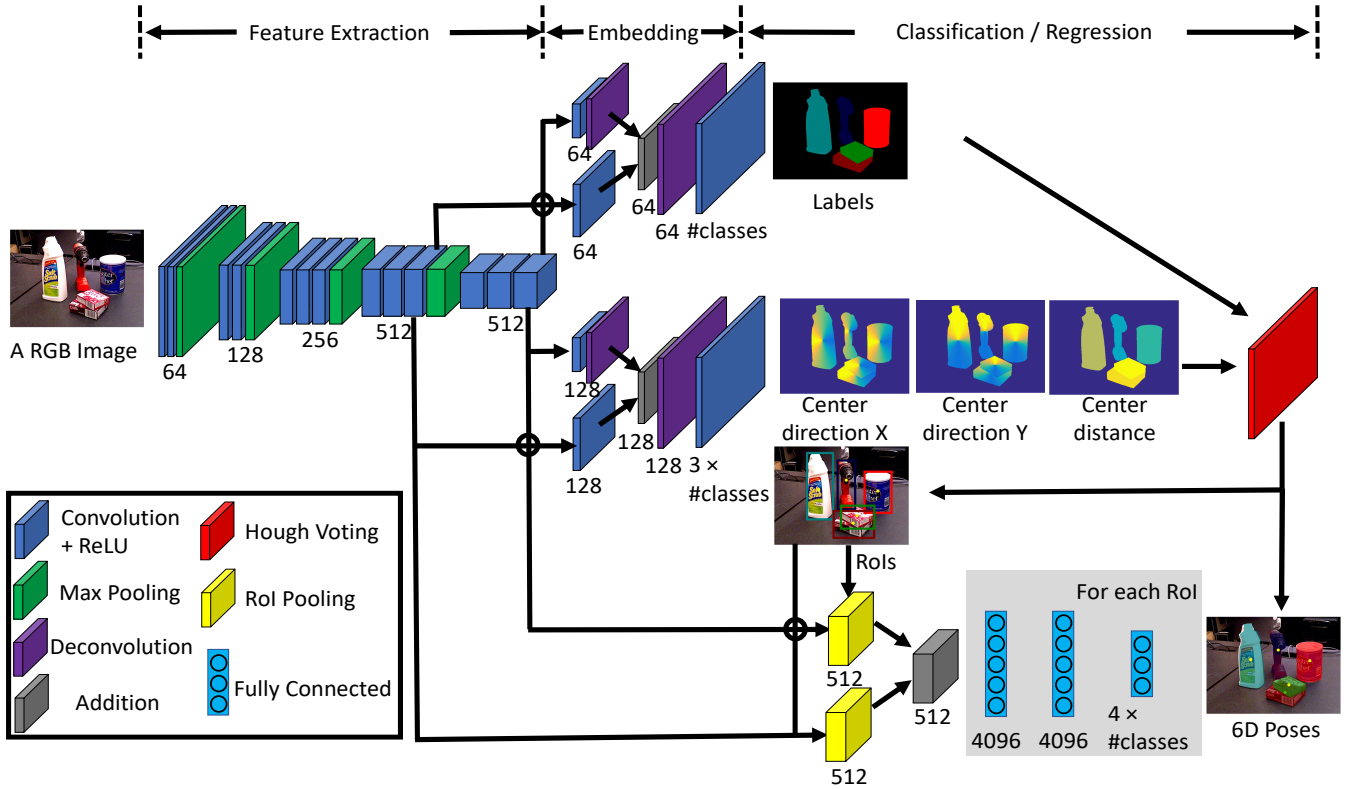


Fig. 2. Architecture of PoseCNNs for 6D object pose estimation.

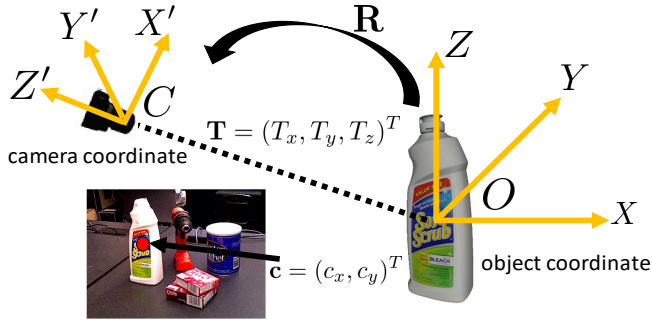


Fig. 3. Illustration of the object coordinate system and the camera coordinate system. The 3D translation can be estimated by localizing the 2D center of the object and estimating the 3D center distance from the camera.

number of the semantic classes. In training, a softmax cross entropy loss is applied to train the semantic labeling branch. While in testing, a softmax function is used to compute the class probabilities of the pixels. The design of the semantic labeling branch is inspired by the fully convolutional network in [18] for semantic labeling. It is also used in our previous work for scene labeling [19].

### C. 3D Translation Estimation

The next task is estimating the object center and its distance. As illustrated in Fig. 3, the 3D translation  $\mathbf{T} = (T_x, T_y, T_z)^T$  is the coordinate of the object origin in the camera coordinate system. Rather than directly regressing to the values of  $\mathbf{T}$ , we decouple the regression problem into 2D object position in the image and object distance from the camera. To see, suppose the projection of  $\mathbf{T}$  on the

image is  $\mathbf{c} = (c_x, c_y)^T$ . If the network can localize  $\mathbf{c}$  on the image and estimate the depth  $T_z$ , we can recover  $T_x$  and  $T_y$  according to the following projection equation assuming a pinhole camera:

$$\begin{bmatrix} c_x \\ c_y \end{bmatrix} = \begin{bmatrix} f_x \frac{T_x}{T_z} + p_x \\ f_y \frac{T_y}{T_z} + p_y \end{bmatrix}, \quad (1)$$

where  $f_x$  and  $f_y$  denote the focal lengths of the camera, and  $(p_x, p_y)^T$  is the principal point. If the object origin  $O$  is the centroid of the object, we call  $\mathbf{c}$  the 2D center of the object.

Inspired by the traditional Implicit Shape Model (ISM) in which image patches vote for the object center for detection [20], we design our network to regress to the center *direction* for each pixel in the image. Specifically, for a pixel  $\mathbf{p} = (x, y)^T$  on the image, it regresses to three variables:

$$(x, y) \rightarrow \left( n_x = \frac{c_x - x}{\|\mathbf{c} - \mathbf{p}\|}, n_y = \frac{c_y - y}{\|\mathbf{c} - \mathbf{p}\|}, T_z \right). \quad (2)$$

Note that instead of directly regressing to the displacement vector  $\mathbf{c} - \mathbf{p}$ , we design the network to regress to the unit length vector  $\mathbf{n} = (n_x, n_y)^T = \frac{\mathbf{c} - \mathbf{p}}{\|\mathbf{c} - \mathbf{p}\|}$ , i.e., 2D center direction, which is scale-invariant and therefore easier to be trained (as we verified experimentally).

The center regression branch of our network (Fig. 2) uses the same architecture as the semantic labeling branch, except that the channel dimensions of the convolutional layers and the deconvolutional layers are different. We embed the high-dimensional features into a 128-dimensional space instead of 64-dimensional since this branch needs to regress to three

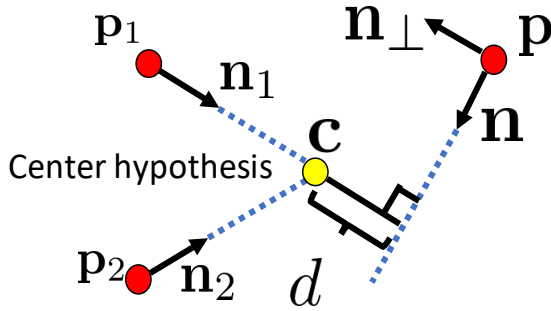


Fig. 4. Illustration of the center hypothesis generation and evaluation in the pre-emptive RANSAC algorithm.

variables for each pixel and each object class. The last convolutional layer in this branch has dimension  $3 \times n$  with  $n$  the number of object classes. In our initial experiments, we found that regressing to a center estimate *for each object* individually performs significantly better than regressing to a single center estimate. In training, a L1 loss function is applied for regression.

In order to find the 2D object center from the pixel-wise semantic labeling results and the center regression results, a Hough voting layer is designed and integrated into the network. It adopts the pre-emptive RANSAC algorithm as in [21] and [11] to handle noise in the results predicted from the network. The pre-emptive RANSAC first samples object center hypotheses. A center hypothesis  $H$  can be determined by sampling a class label and two pixels labeled as belonging to that class. As shown in Fig. 4, the center location  $c$  in the image is computed as the intersection of the two rays cast according to predicted directions  $\mathbf{n}_1$  and  $\mathbf{n}_2$  on the two pixels  $\mathbf{p}_1$  and  $\mathbf{p}_2$  respectively. Intuitively, to determine the quality of a hypothesis, the approach counts the number of pixels belonging to the same class that consistently point toward the center position of the hypothesis. Specifically, a pixel  $\mathbf{p}$  is considered to be an *inlier* of  $H$  if  $\mathbf{p}$  has the same class label as  $H$  and the distance  $d$  from center  $c$  to the ray cast from  $\mathbf{p}$  is smaller than a predefined threshold, where

$$d = \frac{|(\mathbf{c} - \mathbf{p})^T \mathbf{n}_\perp|}{\|\mathbf{n}_\perp\|} \quad (3)$$

and  $\mathbf{n}_\perp$  is perpendicular to  $\mathbf{n}$ , *i.e.*, norm direction of the ray.

After generating a set of center hypotheses, they are ranked according to the number of their inliers. Then the lower half of the hypotheses is removed, and the remaining hypotheses are refined using their inliers. Suppose the inliers of hypothesis  $H$  are  $\{\mathbf{p}_i = (x_i, y_i)\}_{i=1}^m$ , where  $m$  is the number of the inlier pixels. Let us denote the center regression results of these inliers by  $\{\mathbf{n}_i, T_z^i\}_{i=1}^m$ , just as in Eq. 2. Then we solve the following least squares problem to find the center location that is close to all the inliers of the hypothesis:

$$\mathbf{c}^* = \arg \min_{\mathbf{c}} \sum_{i=1}^m \frac{|(\mathbf{c} - \mathbf{p}_i)^T \mathbf{n}_{i\perp}|}{\|\mathbf{n}_{i\perp}\|}. \quad (4)$$

The depth prediction of  $H$  is simply the mean of the depths

predicted by the inliers:

$$T_z^* = \frac{1}{m} \sum_{i=1}^m T_z^i. \quad (5)$$

The refinement is repeated until there is only one hypothesis left for each object class, which determines the 2D center location  $c$  and  $T_z$  for that object class. Using Eq. 1, we can estimate the 3D translation  $\mathbf{T}$ . In addition, the network generates the bounding box of the object as the 2D rectangle that bounds all the inliers, and the bounding box is used for 3D rotation regression.

#### D. 3D Rotation Regression

The lowest part of Fig. 2 shows the 3D rotation regression branch. Using the object bounding boxes predicted from the Hough voting layer, we utilize two RoI pooling layers [16] to “crop and pool” the visual features generated by the first stage of the network for the 3D rotation regression. The pooled feature maps are added together and fed into three Fully-Connected (FC) layers. The first two FC layers have dimension 4096, and the last FC layer has dimension  $4 \times n$  with  $n$  the number of object classes. For each class, the last FC layer outputs a 3D rotation represented by a quaternion.

Instead of using Euler angles or a rotation matrix to represent the 3D rotation, we use a quaternion since it is more efficient to compute the angular distance between two 3D rotations. Given two quaternions  $\mathbf{q}_1$  and  $\mathbf{q}_2$ , the angle  $\theta$  of rotation from  $\mathbf{q}_1$  to  $\mathbf{q}_2$  is  $\theta = \arccos(2\langle \mathbf{q}_1, \mathbf{q}_2 \rangle^2 - 1)$ . In training, we use the following distance function as the loss function for the 3D rotation regression:

$$D(\mathbf{q}_1, \mathbf{q}_2) = 1 - \langle \mathbf{q}_1, \mathbf{q}_2 \rangle^2. \quad (6)$$

Note that, Eq. 6 only works for unit quaternions. Therefore, in the network, the output from the last FC layer is normalized before computing the loss.

#### E. Pose Refinement

The 6D pose estimated from our network can be refined when additional inputs are available. When color images from different viewpoints are available, either in the stereo case or multi-view case, we can refine the 3D translations by triangulating the 2D centers of objects on the images. Triangulation is helpful in correcting errors in estimating  $T_z$ , which tends to have larger displacement since estimating depth from a single image is a very challenging task.

When a depth image is available, we use the Iterative Closest Point (ICP) algorithm to refine the 6D pose. Specifically, we use ICP with projective data association and a point-plane residual term. We render a predicted observation given the 3D model and an estimated pose, and assume that each observed depth value is associated with the predicted depth value at the same pixel location. The residual for each pixel is then the smallest distance from the observed point in 3D to the plane defined by the rendered point in 3D and its associated normal. Points with residuals above a specified threshold are rejected and the remaining residuals are minimized using gradient descent.



Fig. 5. The subset of 21 YCB Objects selected to appear in our dataset.

In the multi-view case, if we estimate the camera transformations between the images, we can transform a 6D pose on one image to all the other images. Then each 6D pose is ranked by projecting the 3D model to all the images according to the 6D pose and measuring the compatibility between the projections and the images. When only color is available, the compatibility is measured by the overlap of the projection and the semantic labels. When depth is available, the compatibility is measured by the mean closest distance between the projected points from the 3D model and the 3D points computed from the depth image. Finally, we select the top-ranked 6D pose as the pose estimation for all the images.

#### IV. THE YCB-VIDEO DATASET

Object-centric datasets providing ground-truth annotations for object poses and/or segmentations are limited in size by the fact that the annotations are typically provided manually. For example, the popular LINEMOD dataset [6] provides manual annotations for around 1,000 images for each of the 15 objects in the dataset. While such a dataset is useful for evaluation of model-based pose estimation techniques, it is orders of magnitude smaller than a typical dataset for training state-of-the-art deep neural networks. One solution to this problem is to augment the data with synthetic images. However, care must be taken to ensure that performance generalizes between real and rendered scenes.

##### A. 6D Pose Annotation

Instead of annotating all the video frames manually, we first provide coarse manual annotations for the first frame of a collection of RGB-D videos, then use a model-based tracking system to estimate the camera trajectory and relative poses between objects. This allows us to compute the pose of each object in each individual frame by composing the object-to-world transform and the world-to-camera transform for the frame. A segmentation can also be generated by rendering the 3D model according to the labelled pose. In this way, each of a small number of manual annotations can be used

TABLE I  
STATISTICS OF OUR YCB-VIDEO DATASET

Number of Objects	21
Total Number of Videos	92
Held-out Videos	12
Min Object Count	3
Max Object Count	9
Mean Object Count	4.47
Number of Frames	133,827
Resolution	640 x 480

by the tracker to generate thousands of labelled images. Furthermore, because the annotation for the first frame is not final but simply an initialization for the tracker, it does not need to be nearly as accurate and can therefore be generated much faster than a typical manual annotation.

More specifically, the first frame of each video is labelled by manually specifying which objects are present, then selecting three points on each object and three corresponding points in the images. It is assumed that objects either rest on a planar surface or on other objects; the plane is also estimated, and initialized with another three correspondences. From here, Signed Distance Function (SDF) representations of each object are used to estimate the pose of each object in the first depth frame. Next, the camera trajectory is initialized by fixing the object poses relative to one another and tracking the object configuration through the depth video. Finally, the camera trajectory and relative object poses are refined in a global optimization step.

##### B. Dataset Characteristics

The objects we used are a subset of 21 of the YCB objects [1], selected due to high-quality 3D models and good visibility in depth. The videos are collected using an Asus Xtion Pro Live RGB-D camera in fast-cropping mode, which provides RGB images at a resolution of 640x480 at 30 FPS by capturing a 1280x960 image locally on the device and transmitting only the center over USB. This results in higher effective resolution of RGB images at the cost of a lower FOV, but given the minimum range of the depth sensor this was an acceptable trade-off. The full dataset comprises 133,827 images, two full orders of magnitude larger than the LINEMOD dataset. For more statistics relating to the dataset, see Table I. Fig. 6 shows one annotation example in our dataset where we render the 3D models according to the annotated ground truth pose. Fig. 7 shows an example of a stereo pair generated from our video dataset.

One drawback of our approach to dataset collection is that the accuracy of each annotation suffers from several sources of error, including the rolling shutter of the RGB sensor, inaccuracies in the object models, slight asynchrony between RGB and depth sensors, and uncertainties in the intrinsic and extrinsic parameters of the cameras. However, we hope that our dataset will still prove useful by making up for in scale where it lacks in accuracy. Another drawback is that the frames within one video are highly correlated, as they depict the same objects in a static configuration in a single scene. However, the motion of the camera through the video induces



Fig. 6. **Left:** an example image from the dataset. **Right:** Textured 3D object models (provided with the YCB dataset) rendered according to the pose annotations for this frame.



Fig. 7. An example “stereo” pair, generated by pairing regularly spaced “left” frames with the first succeeding frame for which the tracked camera pose is at least 10 cm distant.

large appearance changes and leads to the observation of a variety of occlusions. As has been shown by the use of data augmentation by random cropping, images that appear nearly identical to a human can be independently valuable in training a deep neural network, and we believe the same effect is in play here.

## V. EXPERIMENTS

In this section, we conduct experiments to evaluate our proposed method for 6D object pose estimation.

### A. Datasets

In addition to our YCB-Video dataset, we also evaluate our method on the OccludedLINEMOD dataset [2] to compare with state-of-the-art 6D pose estimation methods. The authors of [2] selected one video with 1,214 frames from the original LINEMOD dataset [6], and annotated ground truth poses for eight objects in that video: Ape, Can, Cat, Driller, Duck, Eggbox, Glue and Holepuncher. There are significant occlusions between objects in this video sequence, which makes this dataset challenging. In order to train our network, we use the eight sequences from the original LINEMOD dataset corresponding to these eight objects. We also generate 80,000 synthetic images of each object for training.

### B. Evaluation Metrics

Evaluating 6D pose estimation is not a trivial task. In the literature, different evaluation metrics have been proposed. On the OccludedLINEMOD dataset, the average distance metric is used for comparison. Given the ground truth rotation  $\mathbf{R}$  and translation  $\mathbf{T}$  and the estimated rotation  $\tilde{\mathbf{R}}$  and translation  $\tilde{\mathbf{T}}$ , the average distance computes the mean of the pairwise distances between the 3D model points transformed

according to the ground truth pose and estimated pose:

$$\bar{d} = \frac{1}{m} \sum_{\mathbf{x} \in \mathcal{M}} \|(\mathbf{R}\mathbf{x} + \mathbf{T}) - (\tilde{\mathbf{R}}\mathbf{x} + \tilde{\mathbf{T}})\|, \quad (7)$$

where  $\mathcal{M}$  denotes the set of 3D model points and  $m$  is the number of points. The 6D pose is considered to be correct if the average distance  $\bar{d}$  is smaller than a predefined threshold. In the OccludedLINEMOD dataset, the threshold is set to 10% of the 3D model diameter. For symmetric objects such as the Eggbox and Glue, the matching between points is ambiguous for some views. Therefore, the average distance is computed using the closest point distance:

$$\bar{d} = \frac{1}{m} \sum_{\mathbf{x}_1 \in \mathcal{M}} \min_{\mathbf{x}_2 \in \mathcal{M}} \|(\mathbf{R}\mathbf{x}_1 + \mathbf{T}) - (\tilde{\mathbf{R}}\mathbf{x}_2 + \tilde{\mathbf{T}})\|. \quad (8)$$

Using a fixed threshold in computing pose accuracy cannot reveal how a method performs on these incorrect poses with respect to that threshold. Therefore, we vary the distance threshold in evaluating our method on our YCB-Video dataset. In this case, we can plot an accuracy-threshold curve, and compute the area under the curve for pose evaluation.

### C. Implementation Details

PoseCNN is implemented using the TensorFlow library [22]. In training, the parameters of the first 13 convolutional layers in the feature extraction stage and the first two FC layers in the 3D rotation regression branch are initialized with the VGG16 network [23] trained on ImageNet [24]. We first train the semantic labeling branch and the 3D translation estimation branch for 40,000 iterations, and then add the 3D rotation regression branch and train the whole network for 80,000 iterations, where Stochastic Gradient Descent (SGD) with momentum is used for training.

### D. Baselines

**3D object coordinate regression network.** Since the state-of-the-art 6D pose estimation methods mostly rely on regressing image pixels to 3D object coordinates [7], [11], [25], we implement a variation of our network for 3D object coordinate regression for comparison. In this network, instead of regressing to center direction and depth as in Fig. 2, we regress each pixel to its 3D coordinate in the object coordinate system. We can use the same architecture since each pixel still regresses to three variables. Then we remove the 3D rotation regression branch. Using the semantic labeling results and 3D object coordinate regression results, the 6D pose is recovered using the pre-emptive RANSAC as in [11] on RGB-D data.

**Pose refinement.** We experiment and evaluate different ways in refining the initial pose predicted from the network. When depth images are available, we refine the pose using the Iterative Closest Point (ICP) algorithm. When multi-view images are available, we triangulate the 2D object centers predicted from the network to refine the 3D translations, and also select the best 6D pose in a common 3D coordinate system for all the images as described in Sec. III-E.

TABLE II  
6D POSE ESTIMATION EVALUATION ON THE YCB-VIDEO DATASET

Object	RGB			RGB-D		
	PoseCNN	PoseCNN+Stereo	PoseCNN+Multiview	3D Coordinate	PoseCNN+ICP	PoseCNN+ICP+Multiview
002_master_chef_can	81.85	84.69	80.87	90.73	86.59	<b>91.38</b>
003_cracker_box	75.09	56.16	56.21	75.38	85.79	<b>87.67</b>
004_sugar_box	78.32	75.56	74.18	92.50	96.42	<b>97.92</b>
005_tomato_soup_can	83.99	86.07	87.14	92.31	<b>94.88</b>	94.30
006_mustard_bottle	89.81	87.92	90.22	87.65	97.99	<b>98.19</b>
007_tuna_fish_can	82.26	89.97	89.62	90.54	95.63	<b>96.58</b>
008_pudding_box	67.36	72.93	77.70	87.49	76.46	<b>96.54</b>
009_gelatin_box	78.36	89.52	91.44	96.53	<b>98.78</b>	98.46
010_potted_meat_can	82.41	82.82	87.91	88.50	92.12	<b>95.06</b>
011_banana	70.88	69.78	78.65	71.91	91.54	<b>96.23</b>
019_pitcher_base	82.46	78.16	77.92	87.18	95.88	<b>97.36</b>
021_bleach_cleanser	67.11	74.73	79.53	89.58	85.21	<b>93.88</b>
024_bowl	74.08	73.61	70.02	68.04	<b>87.93</b>	87.80
025_mug	72.38	83.86	79.13	<b>83.62</b>	77.08	79.14
035_power_drill	68.32	78.75	87.79	84.25	95.16	<b>96.17</b>
036_wood_block	22.23	49.99	56.94	72.41	57.27	<b>80.19</b>
037_scissors	61.84	77.43	81.56	80.83	91.17	<b>91.27</b>
040_large_marker	50.23	74.97	79.88	89.18	91.64	<b>97.47</b>
051_large_clamp	29.44	45.50	32.84	54.85	75.36	<b>79.63</b>
052_extra_large_clamp	30.60	38.99	30.37	40.24	46.30	<b>60.06</b>
061_foam_brick	83.64	87.17	85.93	87.56	<b>94.90</b>	94.32
ALL	69.99	74.78	75.00	82.42	87.21	<b>90.92</b>

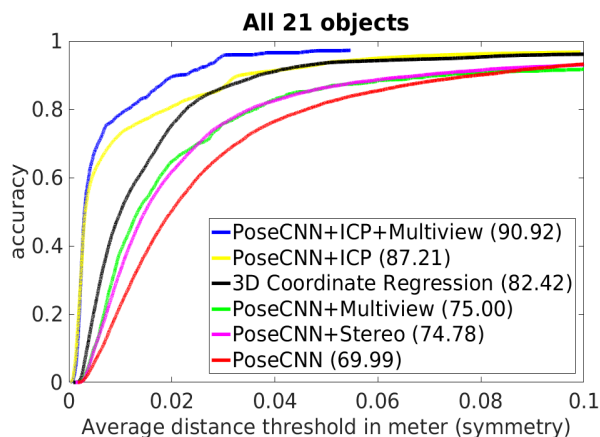


Fig. 8. Accuracy-threshold curves for 6D pose estimation of all the 21 objects in our YCB-Video dataset.

### E. Results on the YCB-Video Dataset

We first evaluate our method on the YCB-Video dataset. In training, we use 80 videos in the dataset and 80,000 rendered images by randomly placing the 21 YCB objects. We test the network on 1,615 stereo pairs generated from the 12 test videos. In Fig. 8, we show the accuracy-threshold curves for 6D pose estimation of all the 21 objects, where we vary the threshold for the average distance using the closest point distance (Eq. 8) and then compute the pose accuracy. The unit of the threshold is meter, and the maximum threshold is 10cm. In the figure, “PoseCNN” indicates our network using RGB only. “PoseCNN+Stereo” and “PoseCNN+Multiview” indicate that the poses from the network are refined with stereo images and multi-view images respectively. “3D Coordinate Regression” shows the result from the network trained for 3D object coordinate regression with RANSAC for 6D

pose estimation on RGB-D data. “PoseCNN+ICP” denotes pose refinement with the closest iterative point algorithm, and “PoseCNN+ICP+Multiview” denotes that the poses after ICP are further refined using multi-view images. The numbers in the legend indicate the percentage of area under each curve, which is used to measure the overall pose accuracy.

We can see that i) stereo triangulation for center locations is helpful, since it is able to refine the 3D translations of the two stereo images. The initial distance estimation of  $T_z$  from the network usually has large error around 5cm. The stereo refinement is able to improve the distance estimation of the translation; ii) Multi-view refinement achieves slightly better performance than using stereo images. iii) 3D coordinate regression network combined with the pre-emptive RANSAC algorithm for 6D pose estimation improves over the stereo and multi-view refinement. The main reason is that the algorithm uses rich depth information about the object 6D pose, rather than using color only; iv) Refining the poses with ICP significantly improves the performance. The pose predicted from our network provides a good initial pose for ICP. With the presence of depth, ICP is able to refine the initial pose well. In addition, we constrain that the pose predicted from ICP to be such that the 2D object center is close to the 2D center estimated by the network. This center constraint prevents ICP from drifting far away from the initial pose. v) By applying multi-view refinement after ICP, we further boost the pose estimation accuracy. Note that depth is also used in the multi-view refinement here.

Table II presents the detailed pose accuracy measured by the percentage of area under the accuracy-threshold curve for each object in the YCB-Video dataset. We can see that some objects are more difficult to handle such as the wood block and the scissors. The network is also confused by the large clamp and the extra large clamp since they have the same

TABLE III  
6D POSE ESTIMATION ACCURACY ON THE OCCLUDEDLINEMOD DATASET

Method	Michel et al. [25]	Hinterstoisser et al. [26]	Krull et al. [2]	Brachmann et al. [7]	Ours 3D Coordinate	Ours PoseCNN+ICP
Ape	80.7	<b>81.4</b>	68.0	53.1	72.3	75.3
Can	88.5	<b>94.7</b>	87.9	79.9	80.6	89.9
Cat	<b>57.8</b>	55.2	50.6	28.2	41.1	56.1
Driller	94.7	86.0	91.2	82.0	<b>94.9</b>	87.4
Duck	74.4	<b>79.7</b>	64.7	64.3	59.1	76.6
Eggbox	47.6	<b>65.5</b>	41.5	9.0	21.2	<b>65.5</b>
Glue	73.8	52.1	65.3	44.5	<b>77.3</b>	73.6
Holepuncher	<b>96.3</b>	95.5	92.9	91.6	64.1	82.1
MEAN	<b>76.7</b>	76.3	70.3	56.6	63.8	75.8

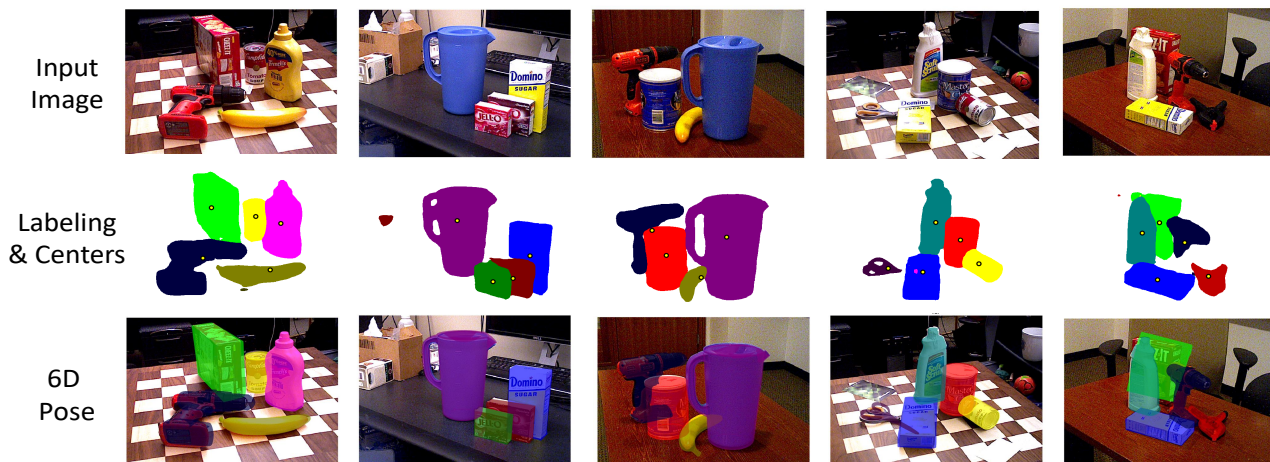


Fig. 9. Examples of 6D object pose estimation results on the YCB-Video dataset using our network with ICP pose refinement.

appearance. The 3D coordinate regression network cannot handle symmetric objects very well such as the banana and the bowl. The performance of the 3D coordinate regression network is worse than our network using color only for the bowl. Another interesting observation is that, the stereo or multi-view refinement may sometimes have large errors if the estimated center location is not accurate such as for the cracker box and the pitcher base. Fig. 9 displays some 6D pose estimation results on the YCB-Video dataset. We can see that the center prediction is quite accurate even in the presence of occlusion between objects, which provides useful constraints in estimating the 6D pose of the object.

#### F. Results on the OccludedLINEMOD Dataset

In order to compare with the state-of-the-art methods for 6D object pose estimation, we conduct experiments on the OccludedLINEMOD dataset. The dataset is challenging due to two aspects. First, there is significant occlusion between objects. Second, the evaluation criterion is strict where a pose is considered to be correct if the average distance is smaller than 10% of the 3D model diameter. The threshold here is usually smaller than 2cm. Table III summarizes the pose estimation results on the OccludedLINEMOD dataset. We can see that our method significantly outperforms [7] and [2]. Compared to the two top-ranked methods [26] and [25], our method with ICP refinement achieves comparable results. We notice that our performance on the Holepuncher is much worse than the four competing methods. This is because we use the point-plane distance in ICP, which cannot refine the

pose well if only a flatten surface of the object is visible as in the holepuncher case. From the table, we can also see that methods which use 3D coordinate regression [25], [2], [7] perform poorly on the Eggbox due to symmetry, while our method is able to handle it well.

## VI. CONCLUSIONS

In this work, we introduce PoseCNN, a convolutional neural network for 6D object pose estimation. PoseCNN decouples the estimation of 3D rotation and 3D translation. It estimates the 3D translation by localizing the object center and predicting the center distance. By regressing each pixel to a unit vector towards the object center, the center can be estimated robustly independent of scale. The 3D rotation is predicted by regressing to the quaternion representation of the 3D rotation using features extracted inside the bounding box of the object. PoseCNN is able to handle symmetric objects as well as occlusion between objects robustly. We also introduce a large scale video dataset for 6D object pose estimation which contains 21 objects in 92 videos with 133,827 frames. We believe that the dataset will be useful for studying 6D object pose estimation in videos, where our results indicate that combining multiple viewpoints can improve detection accuracy.

Our results are extremely encouraging in that they indicate that it is feasible to accurately estimate the 6D pose of objects in cluttered scenes using vision data only. This opens the path to using cameras with resolution and field of view that goes far beyond currently used depth camera systems.

## ACKNOWLEDGMENTS

This work was funded in part by Siemens and by NSF STTR grant 63-5197 with Lula Robotics.

## REFERENCES

- [1] B. Calli, A. Singh, A. Walsman, S. Srinivasa, P. Abbeel, and A. M. Dollar, "The YCB object and model set: Towards common benchmarks for manipulation research," in *International Conference on Advanced Robotics (ICAR)*, 2015, pp. 510–517.
- [2] A. Krull, E. Brachmann, F. Michel, M. Ying Yang, S. Gumhold, and C. Rother, "Learning analysis-by-synthesis for 6D pose estimation in RGB-D images," in *IEEE International Conference on Computer Vision (ICCV)*, 2015, pp. 954–962.
- [3] D. G. Lowe, "Object recognition from local scale-invariant features," in *IEEE international conference on Computer Vision (ICCV)*, vol. 2, 1999, pp. 1150–1157.
- [4] F. Rothganger, S. Lazebnik, C. Schmid, and J. Ponce, "3D object modeling and recognition using local affine-invariant image descriptors and multi-view spatial constraints," *International Journal of Computer Vision (IJCV)*, vol. 66, no. 3, pp. 231–259, 2006.
- [5] A. Collet, M. Martinez, and S. S. Srinivasa, "The MOPED framework: Object recognition and pose estimation for manipulation," *The International Journal of Robotics Research (IJRR)*, vol. 30, no. 10, pp. 1284–1306, 2011.
- [6] S. Hinterstoisser, V. Lepetit, S. Ilic, S. Holzer, G. Bradski, K. Konolige, and N. Navab, "Model based training, detection and pose estimation of texture-less 3D objects in heavily cluttered scenes," in *Asian Conference on Computer Vision (ACCV)*, 2012, pp. 548–562.
- [7] E. Brachmann, A. Krull, F. Michel, S. Gumhold, J. Shotton, and C. Rother, "Learning 6D object pose estimation using 3D object coordinates," in *European Conference on Computer Vision (ECCV)*, 2014, pp. 536–551.
- [8] W. Kehl, F. Milletari, F. Tombari, S. Ilic, and N. Navab, "Deep learning of local RGB-D patches for 3D object detection and 6D pose estimation," in *European Conference on Computer Vision (ECCV)*, 2016, pp. 205–220.
- [9] L. Bo, X. Ren, and D. Fox, "Learning hierarchical sparse features for RGB-D object recognition," *The International Journal of Robotics Research (IJRR)*, vol. 33, no. 4, pp. 581–599, 2014.
- [10] S. Hinterstoisser, C. Cagniard, S. Ilic, P. Sturm, N. Navab, P. Fua, and V. Lepetit, "Gradient response maps for real-time detection of textureless objects," *IEEE Transactions on Pattern Analysis and Machine Intelligence (TPAMI)*, vol. 34, no. 5, pp. 876–888, 2012.
- [11] E. Brachmann, F. Michel, A. Krull, M. Ying Yang, S. Gumhold, and C. Rother, "Uncertainty-driven 6D pose estimation of objects and scenes from a single RGB image," in *IEEE Conference on Computer Vision and Pattern Recognition (CVPR)*, 2016, pp. 3364–3372.
- [12] Z. Cao, Y. Sheikh, and N. K. Banerjee, "Real-time scalable 6DOF pose estimation for textureless objects," in *IEEE International Conference on Robotics and Automation (ICRA)*, 2016, pp. 2441–2448.
- [13] G. Pavlakos, X. Zhou, A. Chan, K. G. Derpanis, and K. Daniilidis, "6-DOF object pose from semantic keypoints," *IEEE International Conference on Robotics and Automation (ICRA)*, 2017.
- [14] C. Rennie, R. Shome, K. E. Bekris, and A. F. De Souza, "A dataset for improved RGBD-based object detection and pose estimation for warehouse pick-and-place," *IEEE Robotics and Automation Letters*, vol. 1, no. 2, pp. 1179–1185, 2016.
- [15] A. Zeng, K.-T. Yu, S. Song, D. Suo, E. Walker, A. Rodriguez, and J. Xiao, "Multi-view self-supervised deep learning for 6D pose estimation in the amazon picking challenge," in *IEEE International Conference on Robotics and Automation (ICRA)*, 2017, pp. 1386–1383.
- [16] R. Girshick, "Fast R-CNN," in *IEEE International Conference on Computer Vision (ICCV)*, 2015, pp. 1440–1448.
- [17] W. Kehl, F. Manhardt, F. Tombari, S. Ilic, and N. Navab, "SSD-6D: Making RGB-based 3D detection and 6D pose estimation great again," in *IEEE Conference on Computer Vision and Pattern Recognition (CVPR)*, 2017, pp. 1521–1529.
- [18] J. Long, E. Shelhamer, and T. Darrell, "Fully convolutional networks for semantic segmentation," in *IEEE Conference on Computer Vision and Pattern Recognition (CVPR)*, 2015, pp. 3431–3440.
- [19] Y. Xiang and D. Fox, "DA-RNN: Semantic mapping with data associated recurrent neural networks," in *Robotics: Science and Systems (RSS)*, 2017.
- [20] B. Leibe, A. Leonardis, and B. Schiele, "Combined object categorization and segmentation with an implicit shape model," in *ECCV Workshop on statistical learning in computer vision*, 2004.
- [21] J. Shotton, B. Glocker, C. Zach, S. Izadi, A. Criminisi, and A. Fitzgibbon, "Scene coordinate regression forests for camera relocalization in RGB-D images," in *IEEE Conference on Computer Vision and Pattern Recognition (CVPR)*, 2013, pp. 2930–2937.
- [22] M. Abadi, P. Barham, J. Chen, Z. Chen, A. Davis, J. Dean, M. Devin, S. Ghemawat, G. Irving, M. Isard, et al., "TensorFlow: A system for large-scale machine learning," in *OSDI*, vol. 16, 2016, pp. 265–283.
- [23] K. Simonyan and A. Zisserman, "Very deep convolutional networks for large-scale image recognition," *arXiv preprint arXiv:1409.1556*, 2014.
- [24] J. Deng, W. Dong, R. Socher, L.-J. Li, K. Li, and L. Fei-Fei, "ImageNet: A large-scale hierarchical image database," in *IEEE Conference on Computer Vision and Pattern Recognition (CVPR)*, 2009, pp. 248–255.
- [25] F. Michel, A. Kirillov, E. Brachmann, A. Krull, S. Gumhold, B. Savchynskyy, and C. Rother, "Global hypothesis generation for 6D object pose estimation," *IEEE Conference on Computer Vision and Pattern Recognition (CVPR)*, 2017.
- [26] S. Hinterstoisser, V. Lepetit, N. Rajkumar, and K. Konolige, "Going further with point pair features," in *European Conference on Computer Vision (ECCV)*, 2016, pp. 834–848.